Featuring I···N halogen bond and weaker interactions in iodoperfluoroalkylimidazoles: An experimental and theoretical charge density study

Alessandra Forni,[*,1] *Davide Franchini,*[2] *Federico Dapiaggi,*[2] *Stefano Pieraccini,*[1,2] *Maurizio Sironi,*[1,2] *Tullio Pilati*[3] *Patrick Scilabra*[3] *Giuseppe Resnati,*[3] *and Yurii L. Yagupolkii*[4]

[1]ISTM-CNR, Istituto di Scienze e Tecnologie Molecolari − Consiglio Nazionale delle Ricerche and INSTM UdR, via Golgi 19, 20133

[2]Department of Chemistry, Università degli Studi di Milano and INSTM UdR, via Golgi 19, 20133 Milano, Italy

[3]NFMLab, DCMIC Politecnico di Milano, via Mancinelli 7, 20131 Milan, Italy

[4]National Academy of Science, Ukraine, Inst. Organic Chem., UA-02094 Kiev, Ukraine

ABSTRACT The experimental charge density distribution of two new iodoperfluoroalkylimidazole derivatives has been determined with the aspherical atom model against single-crystal X-ray diffracted intensities and analyzed by means of the Bader Quantum Theory of Atoms In Molecules. The compounds self-assemble in solid state forming infinite chains through strong I···N halogen bonds. The topological and energetic features of these interactions have been determined and compared with those of a previously reported I···N

interaction formed by a iodoperfluoroarene derivative, allowing to elucidate the role of hybridization of the carbon atom bonded to the halogen atom on the nature of the halogen bonding interaction. The weaker interactions present in the crystal structures have been as well investigated, with particular attention to F···F interactions. They have also been analyzed through the Interacting Quantum Atoms approach in order to elucidate their role in stabilizing the crystal structure.

1. INTRODUCTION

The ability of halogen atoms in haloorganics to attractively interact with Lewis bases, giving rise to the halogen bonding (XB) interaction, is nowadays well documented, as demonstrated by a plethora of either experimental and theoretical investigations or implementations of this interaction for the self-assembling of new functional materials (see Cavallo et al.[1] for a recent and comprehensive review). Research at fundamental level has allowed to explain halogen bonding as a consequence of the anisotropy of the electron density distribution $\rho(\mathbf{r})$ around the halogen atom X covalently bonded to a Y atom. Such anisotropy generates a narrow area of positive electrostatic potential in the region outward X along the Y−X bond direction, the so-called 'σ-hole',[2] which is able to attractively interact with electron donor sites. XB is therefore a predominantly electrostatic interaction, characterized by high directionality in particular if compared with hydrogen bonding, where a much larger area of positive electrostatic potential is hemispherically distributed outward the hydrogen atom.

X-ray charge densities investigations on X···N/O halogen bonded systems[3-9] (X = Cl,[6] Br[5,8,9] and I[3,4,7]), combined with topological analysis of the charge distributions according to the Bader's Quantum Theory of Atoms in Molecules (QTAIM),[10] have provided a clear picture of

the mechanism of halogen bond formation, revealing the presence of a region of charge depletion on the halogen just in the direction of the charge concentration region on the interacting Lewis base. Such complementarity of the charge concentration/depletion sites facing each other in the intermolecular region is further emphasized by the topology of the Laplacian of electron density, $\nabla^2\rho(\mathbf{r})$, in the valence shell of the interacting atoms, as first elucidated by Bader[10] and later made specific for the XB case through formulation of the so-called lump-hole model.[11,12] Atomic regions with positive/negative Laplacian are in fact regions of charge depletion/concentration, a correspondence which is however perfectly observed only for light atoms.[13] For heavier atoms, such as bromine and iodine, a more careful analysis of the Laplacian is generally required to locate the full set of electrophilic and nucleophilic sites on the interacting atoms and in particular cases additional functions should be even used, as recently elucidated by Bartashevich et al. in characterizing the iodine-iodine XB in crystals.[14] In spite of this well-known difficulty, QTAIM was confirmed as a powerful tool to extract meaningful information on both intra- and intermolecular bonding features, allowing in particular to quantitatively compare interactions involving the same pair of atoms in different environments.

Herein we report about an experimental and theoretical charge density investigation on two related iodoalkylimidazoles, IUPAC name (**1**) and … (**2**), which crystallize forming I···N halogen bonded infinite chains. In these structures, the iodine atom is bonded to a perfluorinated alkyl chain, unlike the previously analyzed I···N halogen bonded complex of (E)-1,2-bis(4-pyridyl)ethylene with 1,4-diiodotetrafluorobenzene,[3] hereinafter denoted as **3**, where iodine is bonded to a fluoro-substituted aryl unit. One of the aims of the present investigation was therefore to elucidate the subtle differences in the charge density features of both C–I bonded and I···N non-bonded interactions between the two XB systems involving alkyl vs. aryl iodides.

Two analogous alkyl derivatives have been taken into consideration in order to assess the reproducibility of the experimental findings.

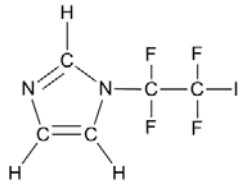

1

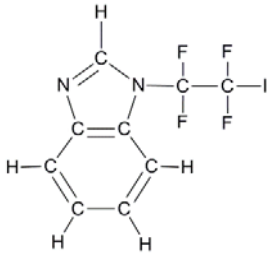

2

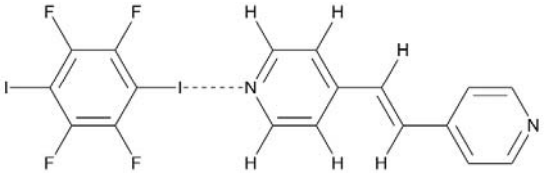

3

An intriguing feature of the crystal structures of **1** and **2** is the large number of F···F contacts below or just above the sum of the fluorine van der Waals radii. The nature of such interactions, which are ubiquitously found in crystal structures of fluorinated molecules and were sporadically characterized in previous charge density studies,[3-5,15,16] has been recently the subject of thorough experimental[17-19] and theoretical[20-23] investigation, after the recognized role of organic fluorine in crystal engineering[24] in spite of its low polarizability. Halogen···halogen ($C–X_1···X_2–C$) contacts are generally geometrically classified[25] according to the values of the two θ_1=$C–X_1···X_2$ and θ_2=$X_1···X_2–C$ angles. Contacts with $\theta_1 \cong \theta_2$, including both *cis* and *trans* geometry when θ_1 and θ_2 differ from 180°, are referred to as type-I, whereas contacts with $\theta_1 \cong 180°$ and $\theta_2 \cong 90°$ are referred to type-II interactions. Type-I interactions are deemed to not have any stabilizing role in crystal structure (when ideally taken alone), while type-II interactions provide a stabilizing electrostatic contribution.[26] A CSD[27] survey to retrieve X···X homohalogen contacts from halogen-substituted hydrocarbons indicates a dominance of type-I over type-II contacts when X is fluorine, unlike what observed for the heavier halogens.[19] This observation suggests that F···F contacts are generally determined by close packing, though the few type-II exceptions

suggest that fluorine can potentially act as the electrophilic species in XB, contributing to govern the crystal packing motif.[19,28]

It is worthwhile to note that, differently from what generally observed for perfluorinated alkyl chains, which tend to be highly disordered in crystal structures at both fluorine and carbon atoms making in some cases altogether impossible to rationalize their statistical disorder,[some ref???29] fluorine atoms in **1** and **2** are unexpectedly highly ordered. Charge density studies were made possible just thanks to this feature, allowing to characterize, for the first time, F···F interactions among perfluorinated alkyl chains.

2. MATERIALS AND METHODS

2.1 Synthesis. xxxxxxxxxxxxxx

2.2 X-ray Diffraction experiments. Single crystals of **1** and **2** suitable for high-resolution X-ray diffraction intensity measurements were grown by slow evaporation from ….. at room temperature. The samples used for data collection have been obtained from shapeless millimetric clusters and, in the case of **1**, successfully sphericized. Diffracted intensities were collected with graphite-monochromated Mo Kα radiation (λ = 0.71073 Å) at a nominal source power of 50 kV × 30 mA on a three-circle Bruker SMART APEX II goniometer equipped with a CCD area detector and an Oxford Cryostream N2 gas blower. The SAINT program package[30] was employed throughout to perform data reductions. Absorption correction was performed with SADABS[31] and the structure was solved with the SHELXS[32] structure solution program using direct methods. In Table 1 we report the details of crystal data and X-ray data collection.

2.3. Refinements and topological analysis of experimental charge densities. Different models have been refined against the observed squared structure factor amplitudes, $|F_o|^2$, by the

VALTOPO program,[33] following the same procedure as previously reported.[5] In Table 2 we summarize the refinement results obtained for **1** and **2** with the conventional independent atom model (IAM), the same model with the inclusion of the third- and fourth-order Gram-Charlier terms on the I atom (IAM + CUM) and the multipole model (POP + CUM). From these data it is evident the importance of including anharmonic parameters on iodine atom and the further improvement associated with the multipolar expansion on all heavy atoms. Atomic anomalous scattering factors were taken from *International Tables for Crystallography* (1995, Vol. C).

In POP + CUM multipole refinement, atomic positions, anisotropic thermal and population parameters of I, F, N and C pseudoatoms, and third- and fourth-order Gram-Charlier coefficients on the iodine atom were varied. On the iodine atom position, functional expansion up to hexadecapole level were introduced, whereas the expansion was broken at octupole level for the other heavy atoms (F, N, C) and at dipole level for the hydrogen atoms. A single parameter was refined for the core of all F, N, and C atoms. The positions of the hydrogen atoms were determined according to the 'polarized hydrogen atoms' approach.[34] During the multipolar refinement of **2**, an extinction correction seemed necessary and an isotropic parameter for a type II crystal, ρ = 0.245(6), was included in the model.[35] The topological analysis of the experimental charge density distributions has been performed with *VALTOPO*.[33] Atomic charges have been obtained by integration of electron density over the topological basins Ω, according to QTAIM.[10] The accuracy of the integration has been estimated through evaluation of the integrated number of electrons (N_Ω), volume (V_Ω), and Laplacian (L_Ω). The corresponding errors, $N_{err}(\%) = (\sum_\Omega m_\Omega N_\Omega - N_{cell})/N_{cell}$, $V_{err}(\%) = (\sum_\Omega m_\Omega V_\Omega - V_{cell})/V_{cell}$ and $L_{err}(\%) = (\sum_\Omega L_\Omega^2/N_{atoms})^{1/2}$, where m_Ω is the site multiplicity for atom Ω, were 0.003, 0.197, 0.062 % and 0.013, 0.201, 0.069 % for **1** and **2**, respectively.

2.4. Quantum Mechanical Calculations. *In vacuo* calculations have been carried out at DFT and, where possible, MP2 levels of theory on both the isolated monomers and dimers of **1** and **2**, using Gaussian09.[36] For DFT calculations, the M06-2X functional[37] has been adopted owing to its optimal performance in treating halogen bonds.[38,39] Moreover, recent investigation[40,41] on the C–X/π halogen bonding involving the aromatic π-electrons system of benzene as electron donor site, revealed that this functional is one of the better choices even to treat dispersion-dominated interactions, which is the case of C–X/π systems in particular when the halogen is chlorine or fluorine. It was also shown that it is able to accurately reproduce not only the binding energies but also the topological properties of such C–X/π weak interactions.[42] These features make the M06-2X functional the optimal choice to treat with comparable accuracy the relatively strong I···N halogen bonding and the weak F···F interactions, which are both the main focus of the present work. The all-electron 6-311++G(d,p) basis set, previously tested for the Br···N interaction,[5] has been used throughout. For the iodine atom this basis set[43] was downloaded from the Basis Set Exchange site.[44] Both single-point (on the experimental geometry) and geometry optimization calculations have been performed. In the case of the dimers, optimization was carried out on the basis set superposition error (BSSE) free potential energy. The topological analysis of the electron density distributions was performed through the AIMALL program.[45]

Solid-state single-point periodic DFT calculations at the T = 100 K experimental geometries of **1** and **2** have been carried out with the Crystal14 program,[46] using the same functional as in the gas-phase calculations and the 6-311G(d,p) basis set. The topological analysis of the electron density distributions obtained by these calculations was performed with the Topond13 program.[47]

3. RESULTS AND DISCUSSION

3.1. Synthesis. xxxxxx

3.2. Structure description. Both compounds **1** and **2** crystallize in the $P2_1/n$ space group with one molecule in the asymmetric unit (see Figures 1 and 2 for partial views of the respective crystal packing diagrams). The bond lengths as obtained by the final multipole refinement (POP + CUM) are collected in Tables S1 and S2 for **1** and **2**, respectively, while Table 3 reports those referring to the C–I bond for **1**-**3**. The crystal structures of **1** and **2** consist of infinite chains in which the molecules are linked by halogen bonding between the iodine atom and the unsubstituted imidazolic nitrogen atom, N1. Several inter-chains C–H···F, C–H···I, C–H···π, F···F and, in the case of **2**, π···π interactions contribute to stabilize the crystal structures. Selected intermolecular contacts (approximately within the sum of the van der Waals radii[48]) are reported in Tables 5 and 6 for **1** and **2**, respectively.

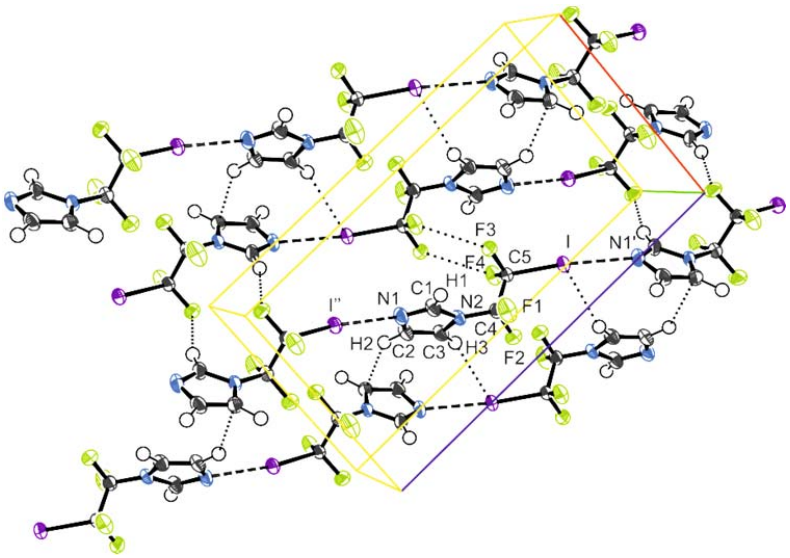

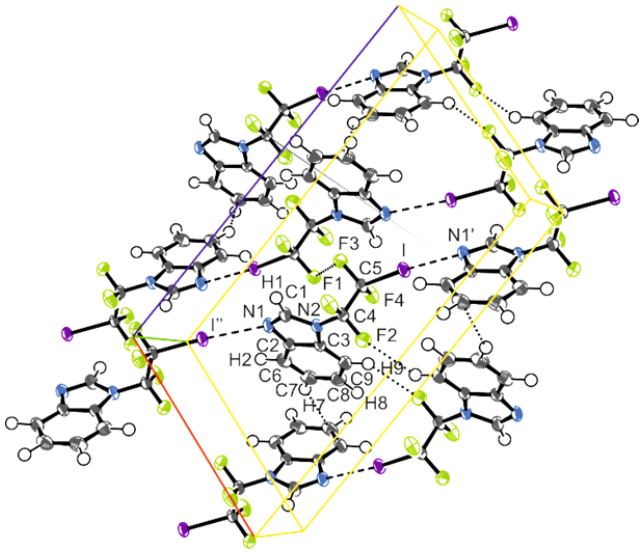

Figure 1. Packing diagrams of **1** (top) and **2** (bottom) at 100 K with atom numbering scheme, showing halogen bonding (dashed lines) and selected weaker interactions (dotted lines). Ellipsoids at 90% probability level.

As expected, the C–I bonds in the present structures (2.1488(4) and 2.1468(4) Å in **1** and **2**, respectively) are slightly longer (by 0.052-0.050 Å) than that of **3**, owing to the different character of the bonded (aliphatic vs. aromatic) carbon atom. Similarly, the I···N1 distances (2.8263(4) and 2.8260(4) Å in **1** and **2**, respectively), though well below the sum of the I and N van der Waals radii (3.53 Å), are longer (by 0.046 Å) than that found in **3**, 2.7804(8) Å, suggesting weaker XB for the former structures. This can be attributed not only to the reduced electrophilicity of the iodine atom bonded to an alkylic chain rather than to an aromatic ring, but also to the lower basicity of the imidazolic nitrogen atom with respect to the pyridinic one. Gas phase geometry optimizations on the monomers of **1** and **2** well reproduce the C–I bond lengths at both DFT and MP2 levels, while those on the corresponding dimers (at DFT and, only for **1**, MP2 levels) significantly overestimate (by about 0.2 Å) the I···N1 distance. According to what previously reported,[5] the latter result is a consequence of the rather flat potential energy surface

between the halogen-bonded partners, which can therefore slightly depart from the geometry of minimum energy owing to crystal packing effects. In agreement, the C5-I···N1 angles, 172.04(2) and 174.56(3)° for **1** and **2**, respectively, are slightly lower than the DFT (178.1 and 178.5 for **1** and **2**, respectively) and MP2 (178.9 for **1**) optimized values.

The final difference Fourier maps ($F_{observed} - F_{multipole}$), calculated in the planes containing halogen bonding and the imidazole rings, are featurless for either systems and the largest peaks are 0.21( ) and 0.27( ) eÅ^{-3} for **1** and **2**, respectively (see Figure 2).

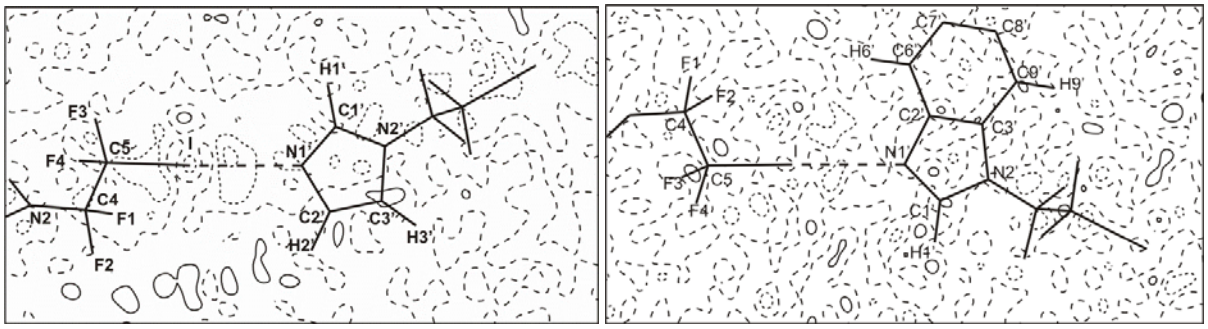

Figure 2. Residual density maps in the least squares plane defined by I, N1', C1' and C2' for **1** (left) and **2** (right) (the prime refers to operations *x-1/2,1/2-y,z-1/2* and *x+1/2,3/2-y,z+1/2* for **1** and **2**, respectively). The contour interval is 0.10 eÅ^{-3}. Solid lines: positive contours, short dashed lines: negative contours, wide dashed lines: zero contours.

3.3. Topological analysis of charge density. The topology of charge density, $\rho(\mathbf{r})$, and its Laplacian, $\nabla^2\rho(\mathbf{r})$, have been analyzed within the quantum theory of atoms in molecules (QTAIM). According to this theory, the existence of a chemical interaction among neighboring atoms is based on the presence of a critical point (bcp) along a line of maximum density (bond path), linking the nuclei of the interacting atoms. At the bcp, the gradient of $\rho(\mathbf{r})$ vanishes and the sign of the Laplacian is determined by the relationship $\nabla^2\rho_{bcp} = \lambda_1 + \lambda_2 + \lambda_3$, where λ_i are the

curvatures of $\rho(\mathbf{r})$ at the bcp. In particular, λ_1 and λ_2 are the two negative curvatures in the directions orthogonal to the bond path and λ_3 is the positive curvature along the bond path. If the electrons are locally concentrated around the bcp and shared by both nuclei, $\nabla^2\rho_{bcp} < 0$ and there is a covalent interaction between the two nuclei. Otherwise, if the electrons are depleted from the bcp and concentrated in each of the atomic basins, $\nabla^2\rho_{bcp} > 0$ and closed shell behavior of the interaction is predicted. An additional criterion for the characterization of the chemical bond is provided by the local electronic energy density $H_b = G_b + V_b$, where G_b and V_b indicate, respectively, the values of the local kinetic and potential energy densities at the bcp. The covalent interactions show negative values of H_b, owing to the dominating V_b contribution, while closed shell interactions exhibit positive values of H_b, since G_b is greater than $|V_b|$.

Figure 3 shows the experimental Laplacian of electron density for **1** and **2** in the plane containing the I···N halogen bond and the aromatic system. The Laplacian maps clearly reveal the different nature of the shared-shell (C–C, C–N, C–H and C–F bonds) and essentially closed-shell (C–I bond and I···N XB) interactions in the two systems.

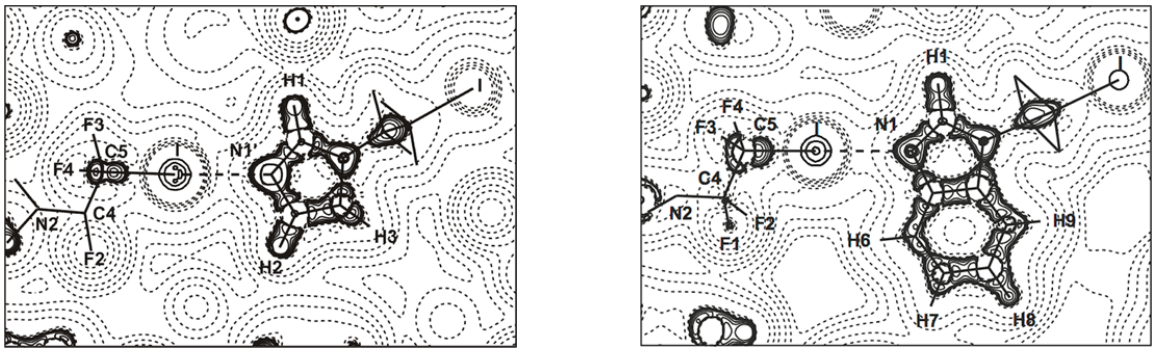

Figure 3. Laplacian of the experimental electron density distribution, $\nabla^2\rho(\mathbf{r})$, of **1** (left) and **2** (right) in the same planes as in Figure 2. The absolute values of the contours (au) increase in

steps of 2×10^n, 4×10^n, and 8×10^n with n beginning at -3 and increasing in steps of 1. Positive values are denoted by dashed contours, negative values are denoted by solid contours.

The topological properties at the bcp's of all covalent bonds as obtained by both the POP+CUM refinement and theoretical (both gas-phase and solid state) calculations are reported in Tables S1 and S2, while those specifically referring to the C–I bond are reported in Table 3. Compared with typical covalent bonds, the C–I bonds in **1**-**3** are characterized by rather low values of ρ_{bcp} and low and positive values of $\nabla^2\rho_{bcp}$, indicating a closed-shell character for this interaction. Interestingly, similar (within the experimental uncertainty) ρ_{bcp} values are obtained for the C–I bonds in the three systems, though the bond length is significantly longer in the alkylic derivatives with respect to the arylic one, which would have suggested reduced strength for the former. Such finding could be ascribed to some effect of crystal packing, which then appear to influence not only intermolecular interactions, as expected (see below), but also specific intramolecular bonds. The importance of the crystal environment on the C–I bond comes out also from a comparison between gas-phase and solid-state calculations. In fact, the former (see second and third row of Table 3 for **1** and **2**) slightly overestimate the electron density at the C–I bcp and provide a negative (though small in magnitude) $\nabla^2\rho_{bcp}$ value, suggesting a stronger bond with some degree of covalence which is not predicted by experiment. The experimental topological features of the C–I bond are however fully recovered when the experimental bond length and the crystal environment are taken into account by periodic calculations (see fourth row of Table 3).

The topological properties at the bcp of the I···N halogen bond in the three structures are collected in Table 4 (see Tables S3 and S4 for those of all intermolecular interactions approximately within the van der Waals radii). As previously described,[3] such halogen bond is a

closed-shell interaction (owing to the positive sign of $\nabla^2\rho_{bcp}$) with a partial shared-shell character (because of the negative sign of H_{bcp}/ρ_{bcp}), unlike the Br···N halogen bond having positive H_{bcp}/ρ_{bcp}.[5] By comparing the topological properties derived for the three iodinated systems, it is however evident the substantially different character of the I···N XB in **1** and **2** (showing virtually the same topological properties) with respect to **3**. The longer XB distance in **1** and **2** is in fact associated with significantly lower ρ_{bcp} and H_{bcp}/ρ_{bcp} (in magnitude) values, indicating weaker interaction with lower shared-shell character for the alkylated iodo-derivatives owing to both intrinsic and extrinsic factors, as elucidated above. Theoretical analysis on the gas-phase XB dimers of **1** and **2** provides lower ρ_{bcp} and positive H_{bcp}/ρ_{bcp} values for the I···N interaction, mainly as a consequence of the longer I···N distances as obtained without including the crystal environment. In fact, periodic calculations at the experimental geometry allow topological properties to get closer to the experimental ones.

3.4. F···F intermolecular interactions.

Both structures **1** and **2** reveal the presence of several F···F interactions, besides other weak interactions such as C-H···I, C-H···F and C-H···π hydrogen bonds and π-π interactions (see Tables S3 and S4). In spite of the large number of F···F interactions, covering a large range of θ_1, θ_2 angles (see Table S5), they result in all cases to be very weak interactions, owing to the low values of ρ_{bcp}, with pure closed shell character, due to the positive values of $\nabla^2\rho_{bcp}$ and H_{bcp}/ρ_{bcp}. As an example of such interactions, we report in Figure 4 a plot of the experimental Laplacian of **1** in the least-squares plane through atoms C4, F1 and C5', F4', featuring the closed shell nature of the F1···F4' interaction. The rather random reciprocal disposition of the interacting fluorine atoms in **1** and **2** is clearly indicative of the close packing origin of all the F···F interactions in

the present structures, differently from the few type-II electrostatic F···F interactions reported in the literature.[19]

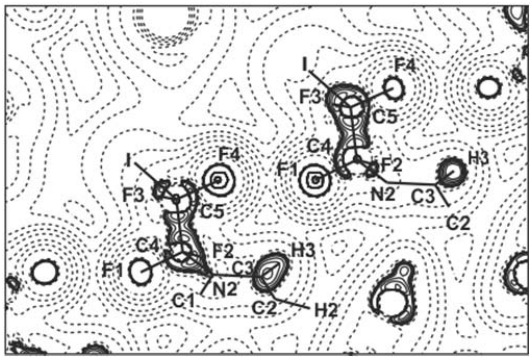

Figure 4. Laplacian of the experimental electron density distribution, $\nabla^2\rho(\mathbf{r})$, of **1** in the least-squares plane of atoms C4, F1, F4', C5'(the prime refers to operation *x,1+y,z*). The absolute values of the contours (au) increase in steps of 2×10^n, 4×10^n, and 8×10^n with *n* beginning at -3 and increasing in steps of 1. Positive values are denoted by dashed contours, negative values are denoted by solid contours.

It is however to be recalled[49] that the presence of a bond path connecting two atoms indicates that the underlying pairwise interaction is anyway stabilizing, even when electrostatic (i.e., classic) repulsive contributions, such as those arising between close fluorine atoms, are dominating. The bond path is in fact associated with a privileged electron-exchange (i.e., quantum mechanical) channel which contributes to lower the mutual interatomic interaction energy. In order to elucidate this aspect an interacting quantum atoms (IQA) analysis[50] has been performed on two representative dimers extracted from the crystal structure, for which F···F bond paths have been found. Based on the QTAIM partition scheme, such analysis allows to decompose the total energy of a many-electron system into monoatomic and diatomic contributions. In particular, for a generic atomic pair AB, the latter term (E_{int}^{AB}) can be expressed

as the sum of nuclear-nuclear (V_{nn}^{AB}), electron-nuclear (V_{en}^{AB}) and electron-electron (V_{ee}^{AB}) interaction energies. V_{ee}^{AB} can further be decomposed into classical (electrostatic, $V_{ee,cl}^{AB}$) and quantum (exchange-correlation, V_{xc}^{AB}) terms, so that:

$$E_{int}^{AB} = V_{cl}^{AB} + V_{xc}^{AB} \quad (1)$$

where $V_{cl}^{AB} = V_{nn}^{AB} + V_{en}^{AB} + V_{ne}^{AB} + V_{ee,cl}^{AB}$. It should be stressed that E_{int}^{AB} refers to the interaction energy between atoms A and B, well distinct from either the energy associated with the formation of the dimer interacting through the A···B contact, and the total interaction energy obtained as the difference between the energies of the dimer and the isolated monomers.[22,51] The IQA analysis has been performed on the dimers interacting through the F1^{I}···F4 (dimer 1) and the F2···F4^{II} (dimer 2) close contacts (see Figure 5 for the related molecular graphs). The first dimer is representative of a type-I F···F contact while the second one is close to a type-II interaction from a geometrical point of view.[25] The three terms of eq. (1) as obtained from such analysis are reported in Table 5 for the full body of atom pairs connected by a bond path in the investigated dimers.

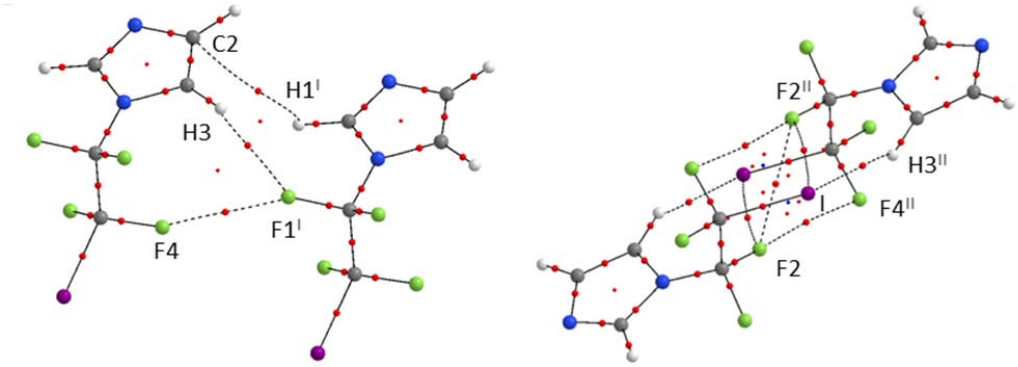

Figure 5. M06-2X/6-311++G(d,p) molecular graphs of dimer 1 (left) and dimer 2 (right) of compound **1** extracted from crystal structure.

As expected, all the reported F···F contacts, independent on their relative disposition, have E_{int}^{AB} positive due to the large electrostatic V_{cl}^{AB} term, denoting destabilizing interactions. On the other hand, the H3···F1^{I} and H3^{II}···I contacts (associated with C–H···X hydrogen bonds) are stabilizing interactions, though only the former has negative and quite high electrostatic contribution, in agreement with its more favorable geometry. It is however to be noted that all F···F contacts have non-negligible exchange-correlation V_{xc}^{AB} contribution, which explains the presence of a bond path[49] and, interestingly, is larger the greater is the value of ρ_b, independent on V_{cl}^{AB}. It is finally to be remarked that the additional C2···H1^{I} and I···F2^{II} interactions (italicized in Table 5), associated with strongly distorted C–H···π hydrogen bond and X···X' XB, respectively, are not observed in the experimental charge density distribution, so that their meaning is questionable being most probably a consequence of neglecting the crystal environment.

3.5. Atomic charges.

Atomic net charges have been determined in **1** and **2** through integration of electron density over the topological atomic basins Ω, at both experimental and theoretical (from gas-phase calculations over the optimized isolated molecules and XB dimers) levels. Their values are reported in Tables S9 and S10. Iodine is characterized by a positive net charge (q = 0.22(2) and 0.28(2) e for **1** and **2**, respectively), well reproduced by theoretical calculations on the monomers (0.20 e in both structures) and even better on the XB dimers (0.28 and 0.27 e for **1** and **2**, respectively, for the iodine involved in the XB interaction). Moreover, calculations on the dimers allow to estimate the intermolecular charge transfer, if any, associated with the XB formation, by summing the atomic charges over the 'donor' and 'acceptor' moieties of the XB dimer. It results that the charge transfer is about 0.02 e in both compounds, then significantly lower than that

computed in the XB dimer of **3**, 0.08 e, in agreement with the stronger interaction detected in the latter system. On the other side, experimental determination of the molecular dipole moment by summing the integrated atomic dipoles provides the values 4.2(5) and 5.8(9) D for **1** and **2**, respectively, which are larger than those computed for the gas-phase optimized molecules (2.40 and 1.99 D at M06-2X, and 2.55 and 2.22 D at MP2 levels for **1** and **2**, respectively) by about 65-75 and 190-160 % (according to the theoretical method), respectively. This enhancement of the dipole moment denotes large polarization effects of the molecules within the XB chain, which is mainly due to the crystal matrix effects because the geometrical variations from gas-phase to solid-state induce only negligible changes (from 2.40/2.55 to 2.75/2.78 D in **1** and from 1.99/2.22 to 2.34/2.47 D in **2**, according to the M06-2X/MP2 method).

3.6. Interaction Energies.

The halogen bonding interaction energy, ΔE, in **1** and **2** has been evaluated through M06-2X/6-311++G(d,p) calculations as the difference between the energy of the XB dimer, optimized on the BSSE-free potential energy surface, and the sum of the energies of the optimized monomers. The ΔE values, -5.7 and -5.5 kcal/mol for **1** and **2**, respectively, are smaller than that reported for **3**, though computed at lower level of theory, amounting to 6.5 kcal/mol, in agreement with what deduced on the basis of the topological properties at the I···N bcp of the three structures. A crude estimation of the XB interaction, based on the Espinosa-Molins-Lecomte (EML) formula $E_{int} = 0.5V_{bcp}$[52] as derived for O···H hydrogen bonds and actually referring to interatomic rather than intermolecular interactions, provides E_{int} = -7.4, -7.0 and -8.9 kcal/mol for **1**, **2** and **3**, respectively, using the experimental V_{bcp} values. For the halogen bonded molecular pair, such E_{int} *interatomic* energies could be directly compared with the ΔE

intermolecular ones because only one bcp is found between the two interacting molecules. While it is clear that a local topological descriptor such as V_{bcp} does not necessarily correlate with the intermolecular interaction energy ΔE, it is however interesting to note that using the approximate 'universal' relationship depicted by Spackman,[53] which connects the EML atom-atom interaction energies for a given atom···atom pair with the interatomic distance d, namely $E_{int} = -3.30 \exp(-2.669[d - d_{vdW}]/\text{Å})$ kJ mol^{-1}, d_{vdW} being the sum of vdW radii, we get $E_{int} = -5.2$ kcal/mol for both **1** and **2**, and −5.8 kcal/mol for **3**. These values are much closer to the computed ΔE results with respect to those derived by directly applying the EML formula and, in the case of **3**, the Spackman E_{int} is in better agreement with the previously reported interaction energy, 5.0 kcal/mol, as obtained by calculations based on the Gavezzotti's PIXEL approach on the XB molecular pair of **3**.[54] Moreover, using the full set of 28 V_{bcp} values for the intermolecular contacts in **1** and **2**, the log-linear plot of EML values, $-E_{int}$, vs. the internuclear distances minus the sum of vdW radii (see Figure 6 and Table S11) provides a line of best fit $E_{int} = -3.57 \exp(-2.384[d - d_{vdW}]/\text{Å})$ kJ mol^{-1}, i.e., very close to that reported by Spackman.[53]

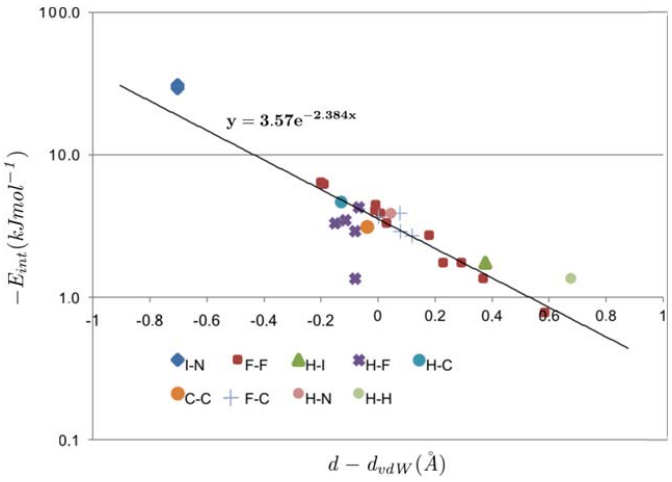

Figure 6. Log-linear plot of EML interatomic interactions ($-E_{int}$), vs internuclear distance (d) minus the sum of van der Waals radii (d_{vdW}). The black line is the best fit to the data of **1** and **2**.

4. CONCLUSIONS

Two new iodoalkylimidazole derivatives, able to self-assemble through I···N halogen bond, have been synthesized and their charge density distribution determined by both multipolar refinement against X-ray diffraction data and theoretical (molecular-scale and periodic) calculations. The topological properties of C–I and I···N bonding and non-bonding interactions have been determined according to QTAIM and compared with those previously reported on an I···N complex based on iodoaryl derivative, allowing to infer the effect of hybridization of the carbon atom bound to the XB donor site. The energetic properties of the XB interaction have been as well characterized through both quantum-mechanical and approximated (i.e., based on local topological descriptors) methods. The full set of intermolecular interactions present in the crystal structures have been investigated, and particular attention has been devoted to F···F interactions, which are present in large number in **1** and **2**. Their nature has been explored by a combined use of QTAIM and IQA energy decomposition scheme. It appears that in all cases the F···F interactions are mainly of electrostatic nature, though the stabilizing exchange-correlation energy term is non-negligible, explaining the presence of the associated F···F bcp's.

Table 1. Experimental details for crystals of **1** and **2**.

	1	**2**
Chemical formula	$C_5H_3F_4IN_2$	$C_9H_5F_4IN_2$
Formula weight	293.99	344.05
Dimensions (mm^3)	0.27×0.18×0.09	0.31×0.26×0.25
Colour, habit	colourless, block	colourless, block

Crystal system	monoclinic	monoclinic
Space group	$P2_1/n$	$P2_1/n$
a (Å)	8.8030(13)	10.0833(5)
b (Å)	5.6607(9)	5.9718(3)
c (Å)	16.061(2)	18.1674(9)
β (°)	90.432(8)	105.156(2)
V (Å^3)	800.3(2)	1055.91(18)
Z	4	4
ρ_{calcd}(g cm^{-3})	2.440	2.164
μ (mm^{-1})	4.016	3.062
λ (Å), MoKα	0.71073	0.71073
Scan method	ϕ and ω	ϕ and ω
T (K)	100(2)	100(2)
h,k,l range	–21→21,–14→13,–39→38	–25→23,–15→15,–45→46
$2\theta_{max}$ (°)	123.32	128.80
no. of measured reflns	185312	377638
no. of independent reflns	12513	17853
R_{int}	0.0276	0.0276
Data completeness (%)	98.3	Xxxxx
Intensity decay	0.00	0.00
Absorption correction	multiscan	Multiscan
Transmission factors T_{min}, T_{max}	0.5877, 0.7520	0.2743, 0.3646

Table 2. Refinement details of **1** and **2**.

	1			**2**		
	IAM	IAM+CUM	POP+CUM	IAM	IAM+CUM	POP+CUM

reflections with $\|F_o\|^2>0$		11923			17196	
parameters	122	147	352	166	191	462
R(F)	0.0253	0.0233	0.0211	0.0285	0.0245	0.0219
wR(F)	0.0153	0.0136	0.0110	0.0217	0.0197	0.0175
$R(F^2)$	0.0217	0.0176	0.0135	0.0208	0.0165	0.0114
$wR(F^2)$	0.0285	0.0252	0.0196	0.0367	0.0323	0.0272
S	1.448	1.281	1.003	1.344	1.186	1.006
scale factor	0.989(1)	1.002(1)	1.000(1)	0.993(1)	1.010(1)	0.999(1)
$(\text{shift/e.s.d.})_{max}$	<0.01	<0.01	<0.01	<0.01	<0.01	<0.01

Table 3. Experimental (first row) and computed (gas-phase monomer optimization at M06-2X/6-311++G(d,p), second row, and at MP2/6-311++G(d,p) levels, third row) C–I bond lengths and associated bcp properties of **1**, **2** and **3**.[3] Fourth row: bcp properties from periodic single point calculations at M06-2X/6-311G** level.

X–Y	R	R_x (Å)	R_x/R_e (Å)	ρ_{bcp} (eÅ^{-3})	$\nabla^2\rho_{bcp}$ (eÅ^{-5})	λ_1 (eÅ^{-5})	λ_2 (eÅ^{-5})	λ_3 (eÅ^{-5})
				1				
C5–I1	2.1488(4)	1.0309	0.48	0.776(7)	1.46(6)	–2.86(7)	–2.71(7)	7.03(13)
	2.1477	*1.0503*	*0.49*	*0.833*	*–0.67*	*–3.09*	*–2.99*	*5.41*
	2.1448	*1.0461*	*0.49*	*0.842*	*–0.76*	*–3.18*	*–3.08*	*5.51*
				0.790	1.16	–2.83	–2.78	*6.77*
				2				
C5–I1	2.1468(4)	1.0382	0.48	0.782(9)	1.95(8)	–3.11(9)	–2.96(9)	8.02(16)
	2.1481	*1.0498*	*0.49*	*0.832*	*–0.69*	*–3.09*	*–2.99*	*5.39*
	2.1462	*1.0457*	*0.49*	*0.840*	*–0.79*	*–3.17*	*–3.07*	*5.46*
				0.798	1.10	–2.97	–2.92	*7.00*
				3				
C7–I1	2.0969(7)	1.0660	0.51	0.76(1)	1.4(2)	–1.94	–1.42	4.79

Table 4. Experimental (first row)[a] and, when available, computed (at M06-2X/6-311++G(d,p) level on the geometry-optimized gas-phase dimer, second row, and at periodic M06-2X/6-311G(d,p) level on the experimental geometry, third row) I···N distances and associated bcp properties of **1**, **2** and **3**.[3]

X···Y	R_e /Å	C–X···Y/°	R_x/R_e	ρ_{bcp}/eÅ^{-3}	$\nabla^2\rho_{bcp}$/eÅ^{-5}	G_{bcp}/HÅ^{-3}	V_{bcp}/HÅ^{-3}	H_{bcp}/ρ_{bcp}	$\lvert V_{bcp}\rvert/G_{bcp}$
					1				
I···N1‘	2.8263(4)	172.04 (2)	0.55	0.205(2)	1.897(18)	0.146(1)	–0.159(3)	–0.064(2)	1.091(3)
	2.9973	178.13		0.126	1.328	0.087	–0.081	0.048	0.930
				0.168	1.765	0.120	–0.116	0.024	0.967
					2				
I···N1‘	2.8260(4)	174.56 (3)	0.55	0.198(2)	1.84(2)	0.140(1)	–0.151(3)	–0.056(3)	1.079(3)
	3.0118	178.52		0.122	1.30	0.084	–0.078	0.050	0.928
				0.175	1.65	0.113	–0.110	0.015	0.976
					3				
I···N1‘	2.7804(8)	179.32(4)	0.54	0.236(2)	1.96(2)	0.164(1)	–0.191(3)	–0.114(3)	1.165(3)

[a] The primes refer to the following symmetry operations: *x-1/2,1/2-y,z-1/2* (**1**), *x+1/2,3/2-y,z+1/2* f (**2**) and *1-x, 1-y,-1-z* (**3**).

Table 5. Electron density at bcp (eÅ^{-3}), interatomic distance (Å), θ_1 and θ_2 angles (°) and IQA total (E_{int}^{AB}), electrostatic (V_{cl}^{AB}) and exchange-correlation (V_{xc}^{AB}) interaction energies (kcal mol^{-1}) computed at M06-2X/6-311++G(d,p) level in selected dimers of **1** for pairs of atoms connected by a bond path.[a]

A···B	ρ_{bcp}	$R_{A\cdots B}$	θ_1	θ_2	E_{int}^{AB}	V_{cl}^{AB}	V_{xc}^{AB}
Dimer 1							
F4···F1^{I}	0.050	2.740	155.85	153.98	37.68	41.16	-3.48
H3···F1^{I}	0.042	2.603	114.31	-[b]	-9.71	-7.89	-1.82
C2···H1^{I}	*0.018*	*3.304*	-[b]	*122.55*	*2.86*	*3.59*	*-0.73*
Dimer 2							
F2···F4^{II}	0.016	3.233	174.44	103.30	36.63	37.53	-0.90
F2···F2^{II}	0.036	2.970	125.72	125.72	39.95	42.12	-2.18

I···H3^{II}	0.050	3.071	- [b]	148.42	-2.88	1.72	-4.60
I···F2^{II}	*0.021*	*3.841*	*72.038*	*72.038*	*-13.53*	*-11.91*	*-1.62*

[a]See Figure 5 for the molecular graphs of dimers 1 and 2. In italics the interactions which are not present in the experimental charge density distribution. Symmetry operations: I, *x, y – 1, z*; II, *–x + 1, –y, –z + 2*. [b]Non-significant for this interaction.

ASSOCIATED CONTENT

Supporting Information. Experimental and computed bond lengths and bcp properties of **1** and **2**, results of IQA analysis, atomic net charges.

AUTHOR INFORMATION

Corresponding Author

*Alessandra Forni e-mail: alessandra.forni@istm.cnr.it.

Author Contributions

The manuscript was written through contributions of all authors. All authors have given approval to the final version of the manuscript.

Funding Sources

…….

ACKNOWLEDGMENT

Fruitful discussion with V. Tognetti and L. Joubert is gratefully acknowledged.

REFERENCES

(1) Cavallo, G.; Metrangolo, P.; Milani, R.; Pilati, T.; Priimagi, A.; Resnati, G.; Terraneo G. The Halogen Bond. *Chem Rev.* **2016**, *116*, 2478-2601.

(2) Clark, T.; Hennemann, M.; Murray, J. S.; Politzer, P. Halogen Bonding: The Sigma-Hole. *J. Mol. Model.* **2007**, *13*, 291−296.

(3) Bianchi, R.; Forni, A.; Pilati, T. The Experimental Electron Density Distribution in the Complex of (E)-1,2-Bis(4-pyridyl)ethylene with 1,4-Diiodotetrafluorobenzene at 90 K. *Chem. Eur. J.* **2003**, *9*, 1631–1638.

(4) Bianchi, R.; Forni, A.; Pilati, T. Experimental Electron Density Study of the Supramolecular Aggregation between 4,4'-Dipyridyl-N,N'-dioxide and 1,4-Diiodotetrafluorobenzene at 90 K. *Acta Crystallogr., Sect. B: Struct. Sci.* **2004**, *60*, 559–568.

(5) Forni, A. Experimental and Theoretical Study of the Br···N Halogen Bond in Complexes of 1,4-Dibromotetrafluorobenzene with Dipyridyl Derivatives. *J. Phys. Chem. A* **2009**, *113*, 3403–3412.

(6) Hathwar, V. R.; Gonnade, R. G.; Munshi, B.; Bhadbhade, M. M.; Guru Row, T. N. Halogen Bonding in 2,5-Dichloro-1,4-benzoquinone: Insights from Experimental and Theoretical Charge Density Analysis. *Cryst. Growth Des.* **2011**, *11*, 1855–1862.

(7) Nelyubina, Y. V.; Antipin, M. Yu.; Lyssenko, K. A. Extremely short halogen bond: the nature and energy of iodine–oxygen interactions in crystalline iodic acid. *Mendeleev Commun.* **2011**, *21*, 250–252.

(8) Pavan, M. S.; Pal, R.; Nagarajan, K.; Guru Row, T. N. Characterization of Interactions Involving Bromine in 2,2-Dibromo-2,3-dihydroinden-1-one via Experimental Charge Density Analysis. *Cryst. Growth Des.* **2014**, *14*, 5477–5485.

(9) Pavan, M. S.; Jana, A. K.; Natarajan, S.; Guru Row, T. N. Halogen Bonding and Chalcogen Bonding in 4,7-Dibromo-5,6-dinitro-2,1,3-benzothiadiazole. *J. Phys. Chem. B* **2015**, *119*, 11382–11390.

(10) Bader, R. F. W. Atoms in Molecules: a Quantum Theory. In *International Series of Monographs on Chemistry 22*; Oxford University Press: Oxford, 1990.

(11) Eskandari, K.; Zariny, H. Halogen Bonding: A Lump-Hole Interaction. *Chem. Phys. Lett.* **2010**, *492*, 9−13.

(12) Tognetti, V.; Joubert, L. Electron Density Laplacian and Halogen Bonds. *Theor. Chem. Acc.* **2015**, *134*, 90.

(13) Shi, Z.; Boyd, R. J. The Shell Structure of Atoms and the Laplacian of the Charge Density. *J. Chem. Phys.* **1988**, *88*, 4375–4377.

(14) Bartashevich, E.; Yushina, I.; Kropotina, K.; Muhitdinova, S.; Tsirelson, V. Testing the Tools for Revealing and Characterizing the Iodine–Iodine Halogen Bond in Crystals. *Acta Crystallogr., Sect. B: Struct. Sci.* **2017**, *73*, 217–226.

(15) Bach, A.; Lentz, D.; Luger, P. Charge Density and Topological Analysis of Pentafluorobenzoic Acid. *J. Phys. Chem. A* **2001**, *105*, 7405–7412.

(16) Hibbs, D. E.; Overgaard, J.; Platts, J. A.; Waller, M. P.; Hursthouse, M. B. Experimental and Theoretical Charge Density Studies of Tetrafluorophthalonitrile and Tetrafluoroisophthalonitrile. *J. Phys. Chem. B* **2004**, *108*, 3663–3672.

(17) Chopra, D.; Cameron, T. S.; Ferrara, J. D.; Guru Row, T. N. Pointers toward the Occurrence of C–F···F–C Interaction: Experimental Charge Density Analysis of 1-(4-Fluorophenyl)-3,6,6-trimethyl-2-phenyl-1,5,6,7-tetrahydro-4H-indol-4-one and 1-(4-Fluorophenyl)-6-methoxy-2-phenyl-1,2,3,4-tetrahydroisoquinoline. *J. Phys. Chem. A* **2006**, *110*, 10465–10477.

(18) Hathwar, V. R.; Guru Row, T. N. Charge Density Analysis of Heterohalogen (Cl···F) and Homohalogen (F···F) Intermolecular Interactions in Molecular Crystals: Importance of the Extent of Polarizability. *Cryst. Growth Des.* **2011**, *11*, 1338–1346.

(19) Pavan, M. S.; Durga Prasad, K.; Guru Row, T. N. Halogen bonding in fluorine: experimental charge density study on intermolecular F···F and F···S donor–acceptor contacts. *Chem. Commun.* **2013**, *49*, 7558–7560.

(20) Johansson, M. P.; Swart, M. Intramolecular halogen–halogen bonds? *Phys. Chem. Chem. Phys.* **2013**, *15*, 11543–11553.

(21) Cormanich, R. A.; Rittner, R.; O'Hagan, D.; Bühl, M. Analysis of CF···FC Interactions on Cyclohexane and Naphthalene Frameworks. *J. Phys. Chem. A* **2014**, *118*, 7901–7910.

(22) Tognetti, V.; Yahia-Ouahmed, M.; Joubert, L. Comment on "Analysis of CF···FC Interactions on Cyclohexane and Naphthalene Frameworks". *J. Phys. Chem. A* **2014**, *118*, 9791–9792.

(23) Yahia-Ouahmed, M.; Tognetti, V.; Joubert, L. Halogen–halogen interactions in perhalogenated ethanes: An interacting quantum atoms study. *Comp. Theor. Chem.* **2015**, *1053*, 254–262.

(24) Chopra, D.; Guru Row, T. N. Role of organic fluorine in crystal engineering. *CrystEngComm* **2011**, *13*, 2175–2186.

(25) Ramasubbu, N.; Parthasarathy, R.; Murray-Rust, P. Angular Preferences of Intermolecular Forces around Halogen Centers: Preferred Directions of Approach of Electrophiles and Nucleophiles around the Carbon-Halogen Bond. *J. Am. Chem. Soc.* **1986**, *108*, 4308–4314.

(26) Desiraju, G. R.; Parthasarathy, R. The Nature of Halogen-Halogen Interactions: Are Short Halogen Contacts Due to Specific Attractive Forces or Due to Close Packing of Nonspherical Atoms? *J. Am. Chem. Soc.* **1989**, *111*, 8725–8726.

(27) Groom, C.R.; Bruno, I. J.; Lightfoot, M. P.; Ward, S. C. The Cambridge Structural Database. *Acta Crystallogr., Sect. B: Struct. Sci.* **2016**, *72*, 171–179.

(28) Metrangolo, P.; Murray, J. S.; Pilati, T.; Politzer, P.; Resnati, G.; Terraneo, G. Fluorine-Centered Halogen Bonding: A Factor in Recognition Phenomena and Reactivity. *Cryst. Growth Des.* **2011**, *11*, 4238–4246.

(29)

(30) SAINT

(31) sadabs

(32) Shelxs

(33) Bianchi, R.; Forni, A. *VALTOPO*: a Program for the Determination of Atomic and Molecular Properties from Experimental Electron Densities. *J. Appl. Crystallogr.* **2005**, *38*, 232–236.

(34) Stewart, R. F.; Bentley, J.; Goodman, B. Generalized X-ray Scattering Factors in Diatomic Molecules. *J. Chem. Phys.* **1975**, *63*, 3786–3793.

(35) Becker, P. J.; Coppens, P. Extinction within the Limit of Validity of the Darwin Transfer Equations. I. General Formalisms for Primary and Secondary Extinction and Their Application to Spherical Crystals. *Acta Cryst.* 1974, **A30**, 129–147.

(36) Frisch, M. J.; Trucks, G. W.; Schlegel, H. B.; Scuseria, G. E.; Robb, M. A.; Cheeseman, J. R.; Scalmani, G.; Barone, V.; Mennucci, B.; Petersson, G. A.; Nakatsuji, H.; Caricato, M.; Li, X.; Hratchian, H. P.; Izmaylov, A. F.; Bloino, J.; Zheng, G.; Sonnenberg, J. L.; Hada, M.; Ehara, M.; Toyota, K.; Fukuda, R.; Hasegawa, J.; Ishida, M.; Nakajima, T.; Honda, Y.; Kitao, O.; Nakai, H.; Vreven, T.; Montgomery, J. A., Jr.; Peralta, J. E.; Ogliaro, F.; Bearpark, M.; Heyd, J. J.; Brothers, E.; Kudin, K. N.; Staroverov, V. N.; Kobayashi, R.; Normand, J.; Raghavachari, K.; Rendell, A.; Burant, J. C.; Iyengar, S. S.; Tomasi, J.; Cossi, M.; Rega, N.; Millam, J. M.; Klene, M.; Knox, J. E.; Cross, J. B.; Bakken, V.; Adamo, C.; Jaramillo, J.; Gomperts, R.; Stratmann, R. E.; Yazyev, O.; Austin, A. J.; Cammi, R.; Pomelli, C.; Ochterski, J. W.; Martin, R. L.; Morokuma, K.; Zakrzewski, V. G.; Voth, G. A.; Salvador, P.; Dannenberg, J. J.; Dapprich, S.; Daniels, A. D.; Farkas, Ö.; Foresman, J. B.; Ortiz, J. V.; Cioslowski, J.; Fox, D. J. Gaussian 09, Revision D.01; Gaussian, Inc: Wallingford, CT, 2013.

(37) Zhao, Y.; Truhlar, D. G. The M06 Suite of Density Functionals for Main Group Thermochemistry, Thermochemical Kinetics, Noncovalent Interactions, Excited States, and

Transition Elements: Two New Functionals and Systematic Testing of Four M06-Class Functionals and 12 Other Functionals. *Theor. Chem. Acc.* **2008**, *120*, 215−241.

(38) Kozuch, S.; Martin, J. M. L. Halogen Bonds: Benchmarks and Theoretical Analysis. *J. Chem. Theory Comput.* **2013**, *9*, 1918−1931.

(39) Forni, A.; Rendine, S.; Pieraccini, S.; Sironi, M. Solvent Effect on Halogen Bonding: The Case of the I···O Interaction. *J. Mol. Graphics Modell.* **2012**, *38*, 31−39.

(40) Forni, A.; Pieraccini, S.; Rendine, S.; Gabas, F.; Sironi, M. Halogen-Bonding Interactions with π Systems: CCSD(T), MP2, and DFT Calculations. *ChemPhysChem* **2012**, *13*, 4224−4234.

(41) Forni, A.; Pieraccini, S.; Rendine, S.; Sironi, M. Halogen Bonds with Benzene: An Assessment of DFT Functionals. *J. Comput. Chem.* **2014**, *35*, 386−394.

(42) Forni, A.; Pieraccini, S.; Franchini, D.; Sironi, M. Assessment of DFT Functionals for QTAIM Topological Analysis of Halogen Bonds with Benzene. *J. Phys. Chem. A* **2016**, *120*, 9071−9080.

(43) Glukhovstev, M. N.; Pross, A.; McGrath, M. P.; Radom, L. Extension of Gaussian-2 (G2) theory to bromine- and iodine-containing molecules: Use of effective core potentials. *J. Chem. Phys.* **1995**, *103*, 1878−1885.

(44) Feller, D. The role of databases in support of computational chemistry calculations. *J. Comp. Chem.* **1996**, *17*, 1571−1586; Schuchardt, K. L.; Didier, B. T.; Elsethagen, T.; Sun, L.; Gurumoorthi, V.; Chase, J.; Li, J.; Windus, T. L. Basis Set Exchange: A Community Database for Computational Sciences. *J. Chem. Inf. Model.* **2007**, *47*, 1045−1052.

(45) Keith, T. A. AIMAll, Version 12.05.09; TK Gristmill Software: Overland Park, KS, 2012, http://aim.tkgristmill.com.

(46) Crystal14

(47) Topond13

(48) Bondi, A. van der Waals Volumes and Radii. *J. Phys. Chem.* **1964**, *68*, 441−447.

(49) Martín Pendás, A.; Francisco, E.; Blanco, M. A.; Gatti, C. Bond Paths as Privileged Exchange Channels. *Chem. Eur. J*., 2007, **12**, 9362.

(50) Blanco, M. A.; Martín Pendás, A.; Francisco, E. Interacting Quantum Atoms: A Correlated Energy Decomposition Scheme Based on the Quantum Theory of Atoms in Molecules. *J. Chem. Theory Comput.* **2005**, *1*, 1096-1109.

(51) Syzgantseva, O. A.; Tognetti, V.; Joubert, L. On the Physical Nature of Halogen Bonds: A QTAIM Study. *J. Phys. Chem. A* **2013**, *117*, 8969−8980.

(52) Espinosa, E.; Molins, E.; Lecomte, C. Hydrogen bond strengths revealed by topological analyses of experimentally observed electron densities. *Chem. Phys. Lett.* **1998**, *285*, 170−173.

(53) Spackman, M. A. How Reliable Are Intermolecular Interaction Energies Estimated from Topological Analysis of Experimental Electron Densities? *Cryst. Growth Des.*, **2015**, *15* 5624–5628.

(54) Gavezzotti, A. Non-conventional bonding between organic molecules. The 'halogen bond' in crystalline systems. *Mol. Phys.* **2008**, *106*, 1473−1485.